ISSN 1063-7834, Physics of the Solid State, 2015, Vol. 57, No. 11, pp. 2145–2150. © Pleiades Publishing, Ltd., 2015.
Original Russian Text © D.M. Gokhfel'd, D.A. Balaev, S.V. Semenov, M.I. Petrov, 2015, published in Fizika Tverdogo Tela, 2015, Vol. 57, No. 11, pp. 2090–2094.

SUPERCONDUCTIVITY

Magnetoresistance Anisotropy and Scaling in Textured High-Temperature Superconductor $Bi_{1.8}Pb_{0.3}Sr_{1.9}Ca_2Cu_3O_x$

D. M. Gokhfel'd[a, *], D. A. Balaev[a, b], S. V. Semenov[a, b], and M. I. Petrov[a]

[a] *Kirensky Institute of Physics, Siberian Branch of the Russian Academy of Sciences, Akademgorodok 50–38, Krasnoyarsk, 660036 Russia*

[b] *Siberian Federal University, pr. Svobodnyi 79, Krasnoyarsk, 660041 Russia*

* *e-mail: gokhfeld@iph.krasn.ru*

Received April 27, 2015

Abstract—The magnetoresistance of the textured high-temperature superconductor (HTSC) $Bi_{1.8}Pb_{0.3}Sr_{1.9}Ca_2Cu_3O_x$ + Ag has been studied at different directions of the transport current **I** and external magnetic field **H** with respect to crystallographic directions of HTSC crystallites. When **I** and **H** are oriented along the *ab* planes of crystallites and φ is the angle between **H** and **I**, the anisotropic part of the magnetoresistance follows the functional dependence $\sin^2\varphi$, which is characteristic of vortex flows under Lorentz forces. The magnetoresistance R at **H** parallel to the *c* axis of crystallites (**H** ∥ *c*) is higher than R at **H** ∥ *ab* for both cases of **I** ∥ *c* and **I** ∥ *ab*. The anisotropy coefficient $\gamma \approx 2.3$ has been estimated from the scaling of the dependences $R(H)$ measured at **H** ∥ *c* and **H** ∥ *ab*. The inclusion of the magnetic field induced by the transport current allows scaling of the dependences $R(H)$ at different values of I. A qualitative picture of the current flow along the *c* axis of crystallites in the textured HTSC has been proposed.

DOI: 10.1134/S1063783415110128

1. INTRODUCTION

The large-scale application of wires based on high-temperature superconductors (HTSC) [1–5] requires understanding of the physical picture of the transport current flow in such materials in the presence of a magnetic field. High transport current densities can be achieved in textured materials [5–11]. Due to the HTSC property anisotropy [1, 12], the critical current density j_C along the crystallographic planes *ab* in textured samples significantly exceeds j_C along the *c* axis [7]. The orientation of the external magnetic field **H** also has an effect on j_C [6, 13]. Among classical layered HTSC compounds, bismuth-based superconductors have the largest anisotropy [1, 12]. The critical current and magnetoresistance anisotropy of textured HTSCs Bi2223 + Ag [6–8, 14–16] were previously studied for the cases where the current flows in the *ab* planes of crystallites, and **H** is parallel to the *c* axis or *ab* planes. The magnetoresistance in the case of ***I*** ∥ *c* in textured samples has not yet been studied. Therefore, it is interesting to study the magnetoresistance behavior in textured HTSCs in the case of macroscopic transport current flows in different directions with respect to the crystallographic orientation of HTSC crystallites.

The present paper is devoted to the study of the magnetoresistance of textured composite samples $Bi_{1.8}Pb_{0.3}Sr_{1.9}Ca_2Cu_3O_x$ + Ag; the cases of **I** ∥ *ab* and **I** ∥ *c* were studied at different **H** orientations.

2. SAMPLE PREPARATION AND EXPERIMENTAL TECHNIQUE

The method for texturing ceramic $Bi_{1.8}Pb_{0.3}Sr_{1.9}Ca_2Cu_3O_x$ (hereafter, Bi2223) is based on the use of porous ceramics. The process for producing porous (20–40% of theoretical density) samples is described in [17–19]. Bi2223 crystallites in these samples are 1–2 μm thick and 20–30 μm in linear size and are randomly ordered. Uniaxial pressing in a liquid medium followed by 30–50-h annealing at 830°C [10, 11] results in texturing of Bi2223 crystallites in a bulk material. In this case, crystallite sizes remain the same as in the source porous material. An addition of ultrafine-grained silver allows improvement of the current-carrying capability of a material [19, 20]. In the present work, studies were performed on the textured sample of composition 70 vol % $Bi_{1.8}Pb_{0.3}Sr_{1.9}Ca_2Cu_3O_x$ and 30 vol % Ag. The typical results of scanning electron microscopy for this sample are shown in Fig. 1. Figure 1a shows the surface corresponding to the *ab* planes of crystallites; Fig. 1b shows a fragment of the sample cleavage along the *c* axes of crystallites. Samples were partially characterized in [11]. The

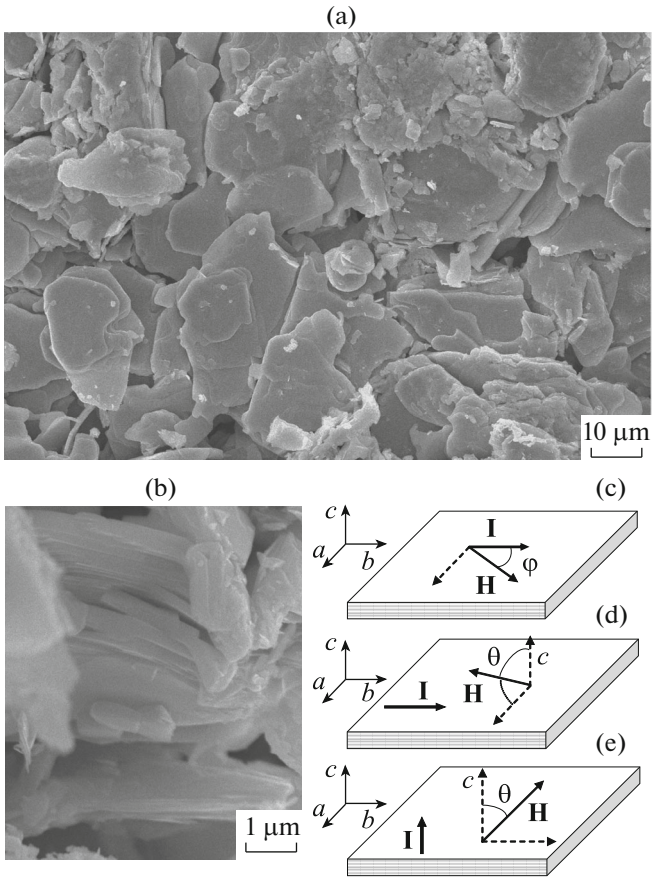

Fig. 1. Micrographs of the textured sample Bi2223 + Ag in the directions (a) parallel to the ab plane and (b) along the *c* axis and (c–e) configurations of **H** and **I** with respect to the crystallographic axes of crystallites, which were used to measure the magnetoresistance.

degree of texture of this sample, determined by the Lotgering method, is 0.98 ± 0.01 (this value is unity for perfect ordering). The critical temperature determined from magnetic measurements is 108 K. The temperature of the transition to the state with "$R = 0$" ($<10^{-6}$ Ω cm) is 106 K. At $T = 77.4$ K, the critical current density is $j_C \approx 220$ A/cm^2 for $\mathbf{I} \parallel ab$. The resistivity ρ at a temperature above the superconducting transition point $T = 113$ K is 0.48 mΩ cm for $\mathbf{I} \parallel ab$ and 0.6 mΩ cm for $\mathbf{I} \parallel c$.

Transport properties were measured by the four-probe method. Electrical contacts were made using Epo-Tek paste. Two contact configurations were used. In the former case, the sample size was 0.25 × 0.15 × 1.0 cm, current contacts were formed on opposite sample end faces, and the stable current I to 1.5 A flowed along the largest sample size. In this configuration, it is expected that the current flows in *ab* planes of Bi2223 crystallites ($\mathbf{I} \parallel ab$). In the latter case, the configuration was similar to that used in ρ_c measurements in single crystals [21]. In this case, the sample was shaped as a square plate 0.4 × 0.4 × 0.16 cm in size. Crystallite *c* axes were perpendicular to the plate. Current contact pads were shaped as square frameworks on opposite sample faces parallel to *ab* planes of Bi2223 crystallites. In empty central space of contact frameworks, potential contacts were formed. In the described configuration, the stable transport current to 3 A flowed along the *c* axis of Bi2223 crystallites ($\mathbf{I} \parallel c$).

The magnetoresistance R was determined as $R(H) = U(H)/I$, where U is the voltage drop. During measurements, the sample was in a liquid nitrogen medium to provide efficient heat removal. The external field **H** was applied at different angles with respect to the crystallographic orientation of Bi2223 crystallites (see schematic images in Figs. 1c–1e). In the case of $\mathbf{I} \parallel ab$, the magnetoresistance measurements were performed for two relative orientations of the magnetic field and the *c* axis of Bi2223 crystallites. In the first case, the angle φ between the external field direction **H** and the current **I** was varied (Fig. 1c). In the second case, the angle θ between the external field direction **H** and the *c* axis of crystallites was varied (Fig. 1d) while retaining the right angle between **H** and **I**. In the case of $\mathbf{I} \parallel c$, the angle θ between **H** and the *c* axis was varied from 0 to 90° (Fig. 1e).

3. RESULTS AND DISCUSSION

3.1. Orientation $\mathbf{I} \parallel ab$, $\mathbf{H} \parallel ab$

Figure 2a shows the dependences of the magnetoresistance $R(H)$ in the case where the current flows in *ab* planes of Bi2223 crystallites, and the external field is parallel or perpendicular to the current and is always parallel to *ab* planes. This configuration is schematically shown in Fig. 1c. Figure 2a shows that the magnetoresistance in the case of $\mathbf{H} \perp \mathbf{I}$ is always higher than for $\mathbf{H} \parallel \mathbf{I}$. The magnetoresistance consists of the contribution R_0 independent of the field direction with respect to current and the anisotropic contribution depending on the angle φ between **H** and **I**. The angular dependence $R(\varphi)$ is well described by the function $R = R_0 + R_L \sin^2\varphi$ (solid lines in Fig. 2b). The anisotropic term is relatively small, $R_L \sim 0.09R_0$.

The obtained dependence $R \sim \sin^2\varphi$ is explained by the Lorentz force action on Abrikosov vortices in the flux creep mode [22]. The small anisotropic contribution R_L suggests that the flux creep under the action of Lorentz forces is not a main mechanism in Bi2223 [23]. Bismuth HTSCs are characterized by low irreversibility fields ($H \sim 2$–4 kOe at $T = 77.4$ K) [24, 25] above which the critical current within crystallites becomes almost zero. Therefore, dissipation processes occur both at crystallite interfaces and in Bi2223 crystallites themselves.

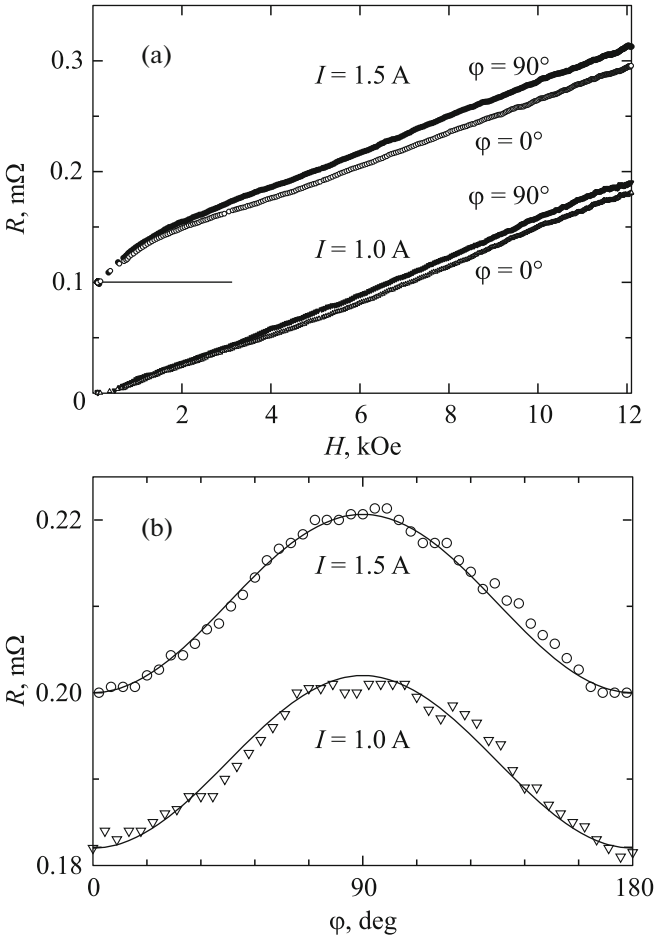

Fig. 2. Magnetoresistance of the sample at $\mathbf{I} \parallel ab$, $\mathbf{H} \parallel ab$. (a) Dependences $R(H)$ at $\varphi = \angle I$, $H = 0$, 90° (curves for $I = 1.5$ A are shifted upward by 0.1 mΩ); (b) dependences $R(\varphi)$ in the field $H = 12.5$ kOe; solid curves are functions $R = R_0 + R_L \sin^2\varphi$.

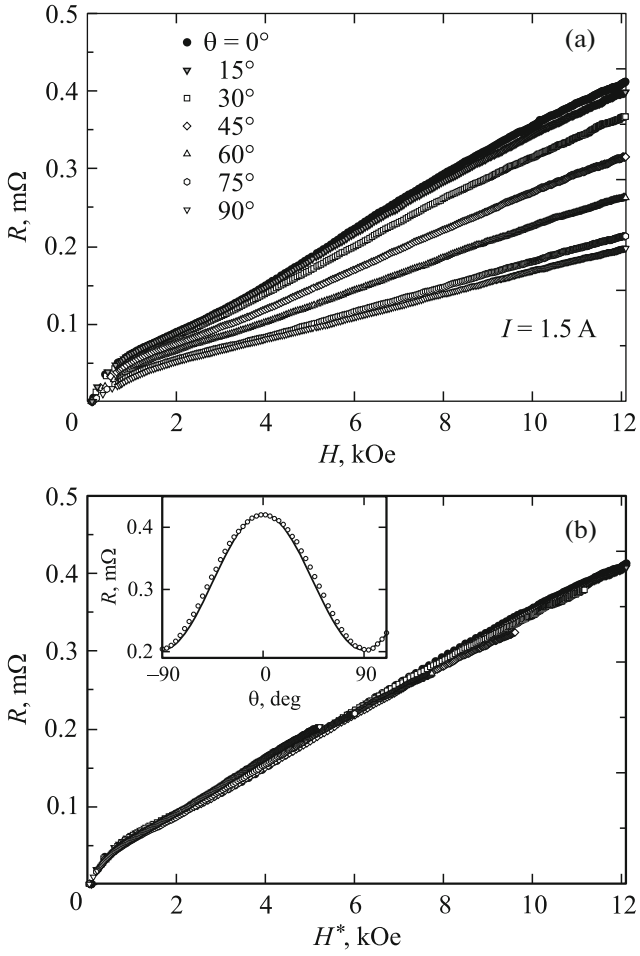

Fig. 3. Magnetoresistance of the sample at $\mathbf{I} \parallel ab$, $\mathbf{H} \perp \mathbf{I}$. Dependences (a) $R(H)$ at different angles $\theta = \angle H$, c and (b) $R(H^*)$ (scaling by expression (1)). The inset shows the dependence $R(\theta)$ in the field $H = 12.5$ kOe; the solid curve is constructed using function (1) (see Subsection 3.2).

3.2. Orientation $\mathbf{I} \parallel ab$, $\mathbf{H} \perp \mathbf{I}$

Figure 3a shows the dependences $R(H)$ (at $\mathbf{I}$ = 1.5 A) for the sample under study at different orientations of $\mathbf{H}$ and the c axis of Bi2223 crystallites. The current flowed along ab planes of crystallites, and the external field was applied at different angles θ between $\mathbf{H}$ and c: from $\mathbf{H} \parallel c$ to $\mathbf{H} \parallel ab$ (see the experimental configuration in Fig. 1d). In this case, the external field is always perpendicular to the transport current.

At such a field orientation, the magnetoresistance of the sample is controlled by the crystallite anisotropy. A change in the field direction with respect to crystallographic axes has an effect on thermodynamic, magnetic, and magnetotransport characteristics of the anisotropic crystal. In [26, 27], it was shown that anisotropic crystal characteristics can be related to equivalent isotropic crystal characteristics independent of field orientation. This equivalent isotropic crystal was considered to be in the effective magnetic field H^* which depends on the orientation of the external field H. The angular dependence of the effective field H^* is given by the expression [26, 27]

$$H^* = H(\gamma^{-2}\sin^2\theta + \cos^2\theta)^{0.5}, \qquad (1)$$

where γ is the anisotropy coefficient. Figure 3b shows the dependences of the magnetoresistance on the effective field H^*, calculated by expression (1) based on the data of Fig. 3a. All dependences $R(H^*)$ coincide at the anisotropy coefficient $\gamma = 2.4 \pm 0.1$. A close value of γ was found for the same scheme of measurements in $(Bi, Pb)_2Sr_2Ca_2Cu_3O_y$ tapes [7]. As shown in [7, 8, 15, 16], non-ideal ordering of crystallites in the textured sample has an effect on the estimated value of γ.

Supposing that $R(H) \sim H$ in strong fields, we can write $R(\theta) = R(H^*) \sim (\gamma^{-2}\sin^2\theta + \cos^2\theta)^{0.5}$. This

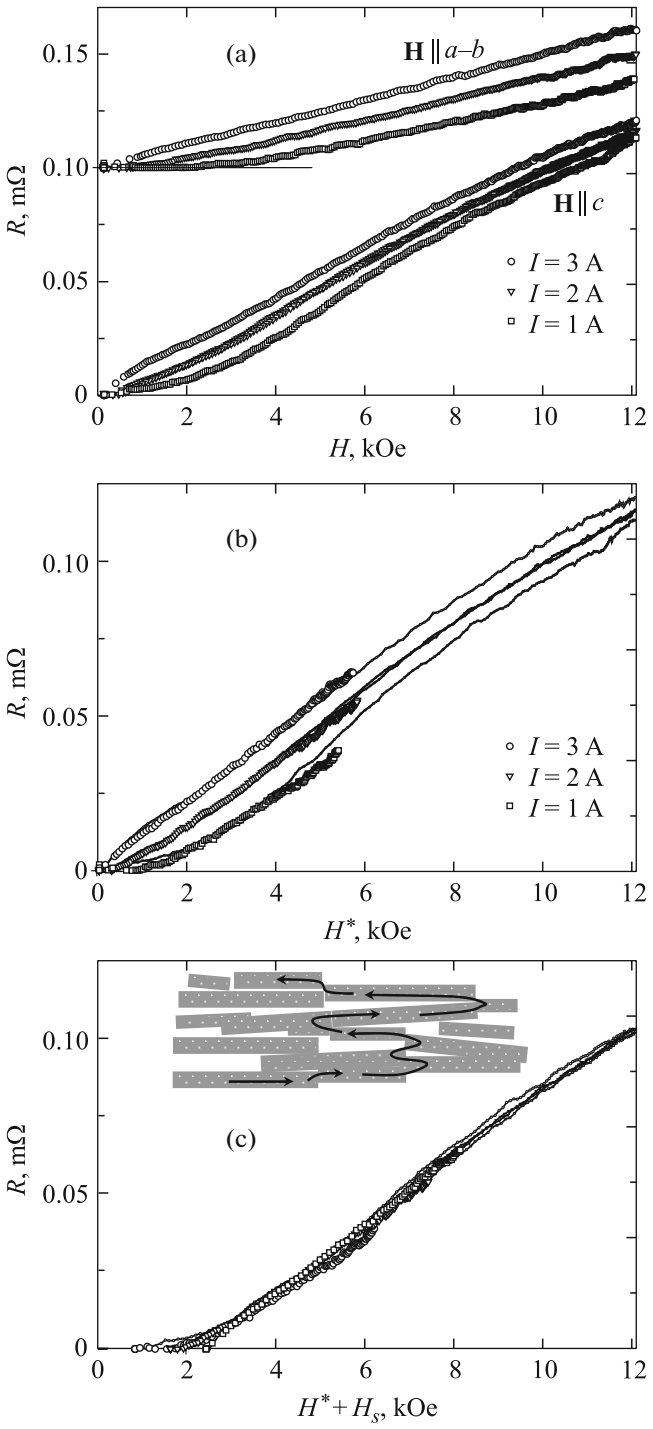

Fig. 4. Magnetoresistance of the sample at $\mathbf{I} \parallel c$. (a) Dependences $R(H)$ (curves for $\mathbf{H} \parallel ab$ are shifted upward by 0.1 mΩ) and (b) their scaling by expression (1) taking into account the effective field H^*; (c) scaling of the same dependences, taking into account the self-field H_s. The inset schematically shows one of the possible trajectories of current flowing over crystallites (see Subsection 3.3).

expression well describes the angular dependence of the voltage drop at fixed values of H and I (see the inset in Fig. 3b).

3.3. Orientation $\mathbf{I} \parallel c$ *in Different* $\mathbf{H}$ *Directions with Respect to the c Axis of Crystallites*

The experimental configuration is shown in Fig. 1e. For the single-crystal sample at such measurement scheme, it is expected that the resistivity will be higher than at $\mathbf{I} \parallel ab$ by the factor γ. At the same time, the magnetoresistance at different $\mathbf{H}$ and c axis orientations can be controlled by both the Lorentz force and crystal anisotropy. However, the resistivities obtained for this case appeared to be of the same order as the resistivity at $\mathbf{I} \parallel ab$ (see Subsection 3.2).

The dependences $R(H)$ of textured Bi2223 in the case where current $\mathbf{I}$ flows in parallel to the c axis at orientations $\mathbf{H} \parallel c$ and $\mathbf{H} \parallel ab$ are shown in Fig. 4a. The transport current densities j and R are of the same order as those measured at $\mathbf{I} \parallel ab$ ($j \sim 20$ A/cm^2 for the data of Fig. 4a at $I = 3$ A and $j \sim 40$ A/cm^2 for the data of Figs. 2a and 3a at $I = 1.5$ A). Hence, the flux creep mode should also be implemented for the studied $\mathbf{H} \parallel c$ orientation. It appeared to be rather unexpected that the magnetoresistance is always significantly higher at orientation $\mathbf{H} \parallel c$ at which $\mathbf{H} \parallel \mathbf{I}$ (Fig. 4a), and the Lorentz force should not affect current transport. At the same time, the dependences $R(H)$ can be scaled similarly to the procedure performed in Subsection 3.2. The dependences $R(H^*)$ for identical transport currents, obtained from the data of Fig. 4a using formula (1), are identical for the anisotropy coefficient $\gamma = 2.25 \pm 0.15$ (Fig. 4b).

Thus, in the case of this experimental scheme, there is no appreciable effect of the Lorentz force, and the results of scaling of the field dependences of the magnetoresistance at different angles θ between $\mathbf{H}$ and c are similar to those described in Subsection 3.2. These observations allow the conclusion that transport current trajectories at the expected orientation $\mathbf{I} \parallel c$ are more complex than those schematically shown in Fig. 1e. Indeed, in the case of strong crystallite anisotropy, the transport current flows mostly along ab planes [8, 14, 28].

Tunneling through crystallite interfaces is also more preferable along ab planes [9] even in the case of good contact along the c axis. Although the contact configuration provides macroscopic currents along the c axis of Bi2223 crystallites (see Section 2), microscopic currents flow in the ab planes of Bi2223 crystallites, which is indicated by the behavior of the dependences $R(H)$. Even weak disordering of crystallites promotes such an increase in the current trajectory length due to preferential flows in ab planes [8, 14, 28].

The schematic representation of current trajectories through the textured HTSC sample is shown in the inset of Fig. 4c, where Bi2223 crystallites are denoted by rectangles whose short side corresponds to the c axis. A similar current flow pattern was considered in [8, 14]. For microscopic currents flowing in ab planes, the orientation $\mathbf{H} \parallel c$ corresponds to the maximum effect of the Lorentz force. This current flow

pattern is additionally confirmed by scaling of the dependences $R(H)$ over the transport current.

The transport current induces a self-magnetic field which affects current–voltage characteristics [13, 29] and magnetoresistance. Therefore, the dependences $R(H^*)$ are different for different currents: at higher transport currents, the magnetoresistance more rapidly increases in weak fields. The self-field H_s of the transport current is taken into account using an analogue of the Silsbee rule [13, 29]: $H_s = gI$, where g is the factor accounting for the sample configuration. For a homogeneous cylindrical sample of radius r and cross section S, coaxial to the field, $g = r/2S = 1/2\pi r$. In the present study, measurements were performed on samples with rectangular cross sections $l \times d$. In this case, the geometrical factor is $g = ld/(l + d)l/2S = 0.5/(l + d)$. Substitution of geometrical sample sizes yields $g = 62.5\ \text{m}^{-1}$. At $I = 1$ A, for such g, the self-field is only 0.8 Oe.

Let us consider a sample in field being a superposition of the effective magnetic field (1) and self-field of the transport current. Figure 4c shows the dependences $R(H^* + H_s)$ obtained from the data of Fig. 4a. The scaled curves well coincide at $g = 6.3 \times 10^4\ \text{m}^{-1}$. At this value, the induced field at a transport current of 1 A is 800 Oe. The significant (by three orders of magnitude) difference of the values of g obtained from geometrical sample sizes and by scaling suggests that the current flows in narrow channels over individual crystallites. Let us estimate the channel section based on the obtained value $g = 6.3 \times 10^4\ \text{m}^{-1}$. Taking the size l equal to the average crystallite thickness of 1 μm, we obtain $d \sim 7$ μm which is comparable to the crystallite size in the ab plane. Scaling of dependences $R(H)$ confirms the proposed model of macroscopic current flows along the c axis of crystallites, according to which microscopic currents flow mostly ab planes.

4. CONCLUSIONS

The magnetoresistance anisotropy of textured HTSC Bi2223 was measured with respect to the directions of the current, magnetic field, and crystallographic axes of crystallites. The angular dependence of the magnetoresistance in the configuration revealing the effect of the Lorentz force is proportional to $\sin^2\varphi$; the contribution of the vortex creep to dissipation is ~9%. The dependences $R(H)$ obtained at different external field directions and the c axis of Bi2223 crystallites are scaled using the expression for the effective field (1) with values $\gamma = 2.25$ for the case of $\mathbf{I} \parallel c$ and $\gamma = 2.4$ for $\mathbf{I} \parallel ab$.

The effect of self-field induced by the transport current on the dependences $R(H)$ was shown.

The analysis of the data on $R(H)$ at $\mathbf{I} \parallel c$ showed that the current flow along the c axis of textured Bi2223 occurs due to microscopic currents flowing in ab planes of crystallites, as is schematically shown in the inset of Fig. 4c.

REFERENCES

1. D. Larbalestier, A. Gurevich, D. M. Feldmann, and A. Polyanskii, Nature (London) **414**, 368 (2001).
2. W. V. Hassenzahl, D. W. Hazelton, B. K. Johnson, P. Komarek, M. Noe, and C. T. Reis, Proc. IEEE **92**, 1655 (2004).
3. A. P. Malozemoff, Annu. Rev. Mater. Res. **42**, 373 (2012).
4. J. X. Jin, Y. Xin, Q. L. Wang, Y. S. He, C. B. Cai, Y. S. Wang, and Z. M. Wang, IEEE Trans. Appl. Supercond. **24**, 1 (2014).
5. O. V. Kharissova, E. M. Kopnin, V. V. Maltsev, N. I. Leonyuk, L. M. Léon-Rossano, I.Yu. Pinus, and B. I. Kharisov, Crit. Rev. Solid State Mater. Sci. **39**, 253 (2014).
6. Q. Y. Hu, R. M. Schalk, H. W. Weber, H. K. Liu, R. K. Wang, C. Czurda, and S. X. Dou, J. Appl. Phys. **78**, 1123 (1995).
7. G. S. Han, Phys. Rev. B: Condens. Matter **52**, 1309 (1995).
8. B. Hensel, G. Grasso, and R. Flükiger, Phys. Rev. B: Condens. Matter **51**, 15456 (1995).
9. G. Desgardin, I. Monot, and B. Raveau, Supercond. Sci. Technol. **12**, R115 (1999).
10. M. I. Petrov, D. A. Balaev, I. L. Belozerova, A. D. Vasil'ev, D. M. Gokhfel'd, O. N. Mart'yanov, S. I. Popkov, and K. A. Shaikhutdinov, Tech. Phys. Lett. **33** (9), 740 (2007).
11. M. I. Petrov, I. L. Belozerova, K. A. Shaikhutdinov, D. A. Balaev, A. A. Dubrovskii, S. I. Popkov, D. A. Vasilyev, and O. N. Martyanov, Supercond. Sci. Technol. **21**, 105019 (2008).
12. S. I. Vedeneev, A. G. M. Jansen, and P. Wyder, Phys. Rev. B: Condens. Matter **67**, 052202 (2003).
13. A. Kilic, K. Kilic, S. Senoussi, and K. Demir, Physica C (Amsterdam) **294**, 203 (1998).
14. J. H. Cho, M. P. Maley, J. O. Willis, J. Y. Coulter, L. N. Bulaevskii, P. Haldar, and L. R. Motowidlo, Appl. Phys. Lett. **64**, 3030 (1994).
15. G. S. Han and C. K. Ong, Phys. Rev. B: Condens. Matter **56**, 11299 (1997).
16. B. Lehndorff, M. Hortig, and H. Piel, Supercond. Sci. Technol. **11**, 1261 (1998).
17. M. I. Petrov, T. N. Tetyueva, L. I. Kveglis, A. A. Efremov, G. M. Zeer, K. A. Shaikhutdinov, D. A. Balaev, S. I. Popkov, and S. G. Ovchinnikov, Tech. Phys. Lett. **29** (12), 986 (2003).
18. K. A. Shaykhutdinov, D. A. Balaev, S. I. Popkov, A. D. Vasilyev, O. N. Martyanov, and M. I. Petrov, Supercond. Sci. Technol. **20**, 491 (2007).
19. M. I. Petrov, D. A. Balaev, I. L. Belozerova, S. I. Popkov, A. A. Dubrovskii, K. A. Shaikhutdinov, and O. N. Mart'yanov, Tech. Phys. **54** (8), 1130 (2009).
20. A. G. Mamalis, S. G. Ovchinnikov, M. I. Petrov, D. A. Balaev, K. A. Shaihutdinov, D. M. Gohfeld, S. A. Kharlamova, and I. N. Vottea, Physica C (Amsterdam) **364–365**, 174 (2001).

21. A. N. Lavrov and L. P. Kozeeva, Physica C (Amsterdam) **248**, 365 (1995).
22. W. K. Kwok, U. Welp, G. W. Crabtree, K. G. Vandervoort, R. Hulscher, and J. Z. Liu, Phys. Rev. Lett. **64**, 966 (1990).
23. K. Kadowaki, Y. Songliu, and K. Kitazawa, Supercond. Sci. Technol. **7**, 519 (1994).
24. D. A. Balaev, S. I. Popkov, S. V. Semenov, A. A. Bykov, K. A. Shaykhutdinov, D. M. Gokhfeld, and M. I. Petrov, Physica C (Amsterdam) **470**, 61 (2010).
25. D. A. Balaev, A. A. Bykov, S. V. Semenov, S. I. Popkov, A. A. Dubrovskii, K. A. Shaikhutdinov, and M. I. Petrov, Phys. Solid State **53** (5), 922 (2011).
26. G. Blatter, V. B. Geshkenbein, and A. I. Larkin, Phys. Rev. Lett. **68**, 875 (1992).
27. Z. Hao and J. R. Clem, Phys. Rev. B: Condens. Matter **46**, 5853 (1992).
28. A. Diaz, J. Maza, and F. Vidal, Phys. Rev. B: Condens. Matter **55**, 1209 (1997).
29. H. Kliem, A. Weyers, and J. Lijtzner, J. Appl. Phys. **69**, 1534 (1991).

Translated by A. Kazantsev